Electronic Supplementary Information (ESI)

Visible-light Excited Luminescent Trigonal Prismatic Metallocages from Template-directed Assembly

Jian-Ping Xu,†[a] Wen Zou,†[a] Shun-Ze Zhan,*[ab] Ji Zheng,[b] Kun Wu,[b] Guo-Hui Zhang,[a]

Jing-Hong Li,[a] Mian Li,[a] Guo-Hong Ning,[b] and Dan Li*[b]

[a] Department of Chemistry and Key Laboratory for Preparation and Application of Ordered Structural Materials of Guangdong Province, Shantou University, Shantou 515063, P. R. China
Email: szzhan@stu.edu.cn

[b] College of Chemistry and Materials Science, and Guangdong Provincial Key Laboratory of Functional Supramolecular Coordination Materials and Applications, Jinan University, Guangzhou 510632, P. R. China *Email: danli@jnu.edu.cn*

† J.-P. Xu and W. Zou contributed equally to this work.

### Content

Section 1: Experimental Section

1.1 Materials and Physical Measurements

Commercially available chemicals were purchased and used without further purification. Infrared spectrum (IR) was obtained in KBr disk on a Nicolet Avatar 360 FTIR spectrometer in the range of 4000–400 cm^{-1}; abbreviations used for the IR bands are: w = weak, m = medium, s = strong, vs = very strong. Elemental analysis (EA) of C, H, N, S was performed with an Elementar Vario EL III CHNS analyzer. ^{1}H-NMR spectroscopy was performed on a Bruker DPX 400 spectrometer using tetramethylsilane (TMS) as internal standard. All δ values are given in ppm. Thermogravimetric analysis (TGA) was performed on a TA Instruments Q50 Thermogravimetric Analyzer under a nitrogen flow of 40 mL·min^{-1} at a heating rate of 10 °C·min^{-1}. Powder X-ray diffraction (PXRD) experiment was performed on a MiniFlex 600 X-ray diffractometer of Riguku Corporation.

The solid-state UV-Vis absorption spectra were recorded on a Lambda950 UV/Vis/NIR spectrophotometer of Perkin Elmer. Steady-state photoluminescence spectra and lifetime were measured with an Edinburgh FLS920 single photon counting spectrometer equipped with a continuous Xe900 xenon lamp, a μF900 μs flash lamp, a red-sensitive Peltier-cooled Hamamatsu R928P photomultiplier tube (PMT), and a closed–cycle cryostat using liquid helium as cooling medium (Advanced Research Systems). The corrections of excitation and emission for the detector response were performed ranging from 200 to 900 nm. The data were analyzed by iterative convolution of the luminescence decay profile with the instrument response function using the software package provided by Edinburgh Instruments. In all cases, the crystalline sample was selected under a microscope with 40-time amplification. The phase purity of the sample is assured by elemental analysis and PXRD measurement.

1.2 Synthesis

1.2.1 Synthesis of ligand *H*L
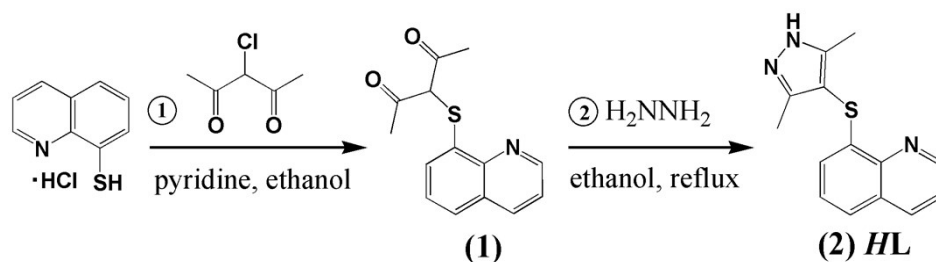
Scheme S1 Synthesis procedure of the ligand *H*L.

The ligand 4-(quinoline-8-thio)-3,5-dimethyl-1H-pyrazole (*H*L) was synthesized according the literature with modifications (**Scheme S1**).[S1]

A mixture of quinoline-8-thiol hydrochloride 0.9884 g (5.0 mmol), 3-chloropentane-2,4-dione 0.6725 g (5.0 mmol), pyridine (2.0 mL) in ethanol (40.0 mL) was stirred at room temperature for 24 h. After cooled to room temperature, the solution was evaporated under reduced pressure to give a white intermediate (1). The intermediate (0.821 g, 4.0 mmol) was then dissolved in ethanol (25 mL), and excess hydrazine hydrate (80%, 0.5 mL, 12.5 mmol) was added with stirring. The mixture was refluxed for 10 h and then cooled. The resulted solution was evaporated under reduced pressure to give faint yellow solid. The solid was recrystallized in ethanol to give faint yellow crystal as *H*L (2). Yield 60%. IR (KBr pellet, cm^{-1}): 3180(s), 3089(s), 2922(s), 2871(s), 1595(s), 1563(m), 1477(m), 1432(s), 1314(w), 1151(w), 1086(w), 1002(m), 846(w), 793(s), 751(m), 680(w), 579(w). ^{1}H NMR (400 MHz, CD$_2$Cl$_2$, Fig. S1) δ 8.98 (dd, J = 4.2, 1.7 Hz, 1H), 8.22 (dd, J = 8.3, 1.7 Hz, 1H), 7.61 (d, J = 8.1 Hz, 1H), 7.52 (dd, J = 8.3, 4.2 Hz, 1H), 7.37 (t, J = 7.8 Hz, 1H), 6.85 (m, 1H), 2.33(s, 6H).

1.2.2 Synthesis of the complexes

(I) One-pot synthesis

A mixture of *H*L (6.40 mg, 0.025 mmol), CuI (9.5 mg, 0.05 mmol) or CuBr (7.20 mg, 0.05 mmol), benzene (**B**, 1.0 mL)/toluene (**MB**, 1.0 mL) in 1.0 mL ethanol or 1,3,5-triphenylbenzene (**TPB**, 5.0 mg, 0.016 mmol) in 2.0 mL ethanol, NH$_3$·H$_2$O (25%, 50 μL) was sealed into a Pyrex tube with 8 mm diameter. Then the tube was heated at 140 °C in a programmable oven for 72 h and cooled to room temperature at the rate of −5

°C/h. Orange column crystals of **B@I**, **MB@I**, **TPB@I**, **B@Br**, **MB@Br** or **TPB@Br** were obtained with yield no more than 15% (based on H**L**).

(II) Step-by-step synthesis

A mixture of H**L** (5.10 mg, 0.02 mmol), CuBr (2.87 mg, 0.02 mmol), DMF (1.0 mL), H_2O (1.0 mL), $NH_3 \cdot H_2O$ (25%, 50 μL) was sealed into a Pyrex tube with 8 mm diameter. Then the tube was heated at 140 °C in a programmable oven for 72 h and cooled to room temperature at the rate of −5 °C/h. Colorless column crystals of complex Cu$_3$**L**$_3$ were obtained in 57% yield (based on H**L**).

A mixture of Cu$_3$**L**$_3$ (7.6 mg, 0.008 mmol), CuI (9.50 mg, 0.05 mmol) or CuBr (7.20 mg, 0.05 mmol), benzene (**B**, 1.0 mL)/toluene (**MB**, 1.0 mL) in 1.0 mL ethanol or 1,3,5-triphenylbenzene (**TPB**, 5.0 mg, 0.016 mmol) in 2.0 mL ethanol, was sealed into a Pyrex tube with 8 mm diameter. Then the tube was heated at 140 °C in a programmable oven for 72 h and cooled to room temperature at the rate of −5 °C/h. Orange column crystals were obtained with yield 35~45% (based on Cu$_3$**L**$_3$).

Results:

Cu$_3$**L**$_3$: Anal. Calcd for $C_{42}H_{36}Cu_3N_9S_3$: C, 52.91; H, 3.78; N, 13.22; S, 10.09; Found: (%): C, 53.04; H, 3.70; N, 13.12; S, 10.01. IR (KBr pellet, cm^{-1}): 3055(m), 2913(m), 1577(s), 1491(vs), 1454(m), 1417(s), 1354(s), 1302(m), 1142(m), 1064(m), 979(m), 819(m), 784(s), 682(w), 654(m), 631(w), 538(m).

B@I: Anal. Calcd for $C_{102}H_{90}Cu_{12}I_6N_{18}S_6$: C, 37.30; H, 2.76; N, 7.68; S, 5.86; Found: (%): C, 37.18; H, 2.55; N, 7.75; S, 5.94. IR (KBr pellet, cm^{-1}): 3022(w), 2955(w), 2912(m), 1580(s), 1492(vs), 1455(m), 1420(s), 1376(s), 1303(m), 1146(m), 1067(m), 1032(m), 985(s), 823(vs), 783(vs), 762(s), 687(vs), 633(w), 535(m).

B@Br: Anal. Calcd for $C_{102}H_{90}Br_6Cu_{12}N_{18}S_6$: C, 40.81; H, 3.02; N, 8.40; S, 6.41; Found: (%): C, 40.90; H, 3.10; N, 8.52; S, 6.30. IR (KBr pellet, cm^{-1}): 3021(w), 2955(w), 2913(m), 1577(s), 1491(vs), 1454(m), 1420(s), 1377(s), 1302(m), 1147(m), 1068(m), 1035(m), 980(s), 822(vs), 781(vs), 760(s), 689(vs), 631(w), 534(m).

MB@I: Anal. Calcd for $C_{105}H_{96}I_6Cu_{12}N_{18}S_6$: C, 37.91; H, 2.91; N, 7.58; S, 5.78; Found: (%): C, 37.99; H, 2.80; N, 7.69; S, 5.65. IR (KBr pellet, cm^{-1}): 3041(w), 2956(w), 2912(m), 2847(w), 1589(s), 1492(vs), 1453(m), 1418(s), 1375(s), 1302(m),

1147(m), 1069(m), 1038(m), 983(s), 825(vs), 782(vs), 764(s), 743(s), 694(m), 633(w), 536(m).

MB@Br: Anal. Calcd for $C_{105}H_{96}Br_6Cu_{12}N_{18}S_6$: C, 41.42; H, 3.18; N, 8.28; S, 6.32; Found: (%): C, 41.31; H, 3.11; N, 8.25; S, 6.39. IR (KBr pellet, cm^{-1}): 3042(w), 2956(w), 2912(m), 2850(w), 1589(s), 1493(vs), 1455(m), 1419(s), 1374(s), 1303(m), 1148(m), 1068(m), 1037(m), 983(s), 825(vs), 784(vs), 764(s), 745(s), 688(m), 633(w), 534(m).

TPB@I: Anal. Calcd for $C_{108}H_{90}I_6Cu_{12}N_{18}S_6$: C, 38.65; H, 2.70; N, 7.51; S, 5.73; Found: (%): C, 38.78; H, 2.61; N, 7.40; S, 5.85. IR (KBr pellet, cm^{-1}): 3054(w), 3040(w), 2958(w), 2913(m), 2848(w), 1590(s), 1492(vs), 1453(m), 1417(m), 1375(s), 1355(m), 1304(m), 1148(m), 1089(m), 1033(w), 981(s), 826(vs), 783(vs), 766(s), 698(m), 633(w), 538(m).

TPB@Br: Anal. Calcd for $C_{108}H_{90}Br_6Cu_{12}N_{18}S_6$: C, 42.19; H, 2.95; N, 8.20; S, 6.26; Found: (%): C, 42.05; H, 2.81; N, 8.32; S, 6.30. IR (KBr pellet, cm^{-1}): 3057(w), 3041(w), 2959(w), 2914(m), 2850(w), 1591(s), 1494(vs), 1455(m), 1419(s), 1373(s), 1356(m), 1304(m), 1150(m), 1070(m), 1038(m), 980(s), 828(vs), 784(vs), 765(s), 700(m), 634(w), 536(m).

Caution! In the synthesis of these complexes, the volume of solution should not exceed one half of the volume of the Pyrex tube to avoid overloading. Be careful of avoiding potential empyrosis and catching fire when flame-sealing.

Section 2: Crystal Data

2.1 Crystal Structure Determination

Suitable crystals were mounted with glue at the end of a glass fiber. Single crystal data of the **G@X** complexes were collected on a Rigaku OD (Enhance Cu X-ray Source, Kα, λ = 1.54178 Å) with CCD Plate (XtaLAB Pro: Kappa single) under a cold nitrogen stream (100 K). Mo X-ray Source (Kα, λ = 0.71073 Å) was used for collecting single crystal data of the Cu_3L_3 complex. The data was processed using CrysAlisPro 1.171.39.28b (Rigaku Oxford Diffraction, 2015). Multi-scan absorptions were applied. Structure were solved by direct methods and refined on F^2 using full-matrix least-squares using SHELXL[S2] within the OLEX2 suite.[S3]

All non-hydrogen atoms were refined with anisotropic thermal parameters, and all hydrogen atoms were included in calculated positions and refined with isotropic thermal parameters riding on the parent atoms. Structural diagrams were produced by using the OLEX computer program.[S4] Crystal data and structure refinement for these complexes are summarized in Table S1. Selected bond lengths and angles are given in Tables S2-5. CCDC nos. 2048251, 2048259, 2048264, 2048269, 2048272, 2048273, 2060347 contain the supplementary crystallographic data for this paper.

2.2 Crystal Data

Table S1 Summary of crystal and structure refinement data for **Cu₃L₃** and **G@X** complexes

	Cu₃L₃	B@I	MB@I	TPB@I	B@Br	MB@Br	TPB@Br
CCDC No.	2060347	2048259	2048269	2048273	2048251	2048264	2048272
Empirical formula	$C_{42}H_{36}Cu_3N_9S_3$	$C_{102}H_{90}Cu_{12}$ $I_6N_{18}S_6$	$C_{105}H_{96}Cu_{12}$ $I_6N_{18}S_6$	$C_{108}H_{90}Cu_{12}$ $I_6N_{18}S_6$	$C_{102}H_{90}Cu_{12}$ $Br_6N_{18}S_6$	$C_{105}H_{96}Cu_{12}$ $Br_6N_{18}S_6$	$C_{108}H_{90}Cu_{12}$ $Br_6N_{18}S_6$
Formula weight	953.60	3284.16	3326.23	3356.22	3002.21	3044.29	3074.28
Temperature (K)	100(2)	100(2)	100(2)	100(2)	100(2)	100(2)	100(2)
Crystal system	Triclinic	Hexagonal	Hexagonal	Hexagonal	Hexagonal	Hexagonal	Hexagonal
Space group	$P-1$	$P6_3/m$	$P6_3/m$	$P6_3/m$	$P6_3/m$	$P6_3/m$	$P6_3/m$
a (Å)	7.4405(2)	17.9429(1)	18.0392(2)	17.9661(1)	17.8011(1)	17.8577(1)	17.8160(2)
b (Å)	15.2059(5)	17.9429(1)	18.0392(2)	17.9661(1)	17.8011(1)	17.8577(1)	17.8160(2)
c (Å)	18.3941(6)	20.5857(2)	20.6238(3)	20.6209(2)	20.0830(2)	20.1981(1)	20.1441(3)
α (°)	110.730(3)	90.00	90.00	90.00	90.00	90.00	90.00
β (°)	93.912(2)	90.00	90.00	90.00	90.00	90.00	90.00
γ (°)	94.630(2)	120.00	120.00	120.00	120.00	120.00	120.00
Volume (Å³)	1929.53(10)	5739.60(7)	5812.11(15)	5764.29(7)	5511.28(8)	5578.17(7)	5537.31(12)
Z	2	2	2	2	2	2	2
ρ_{calc} (g/cm³)	1.641	1.900	1.901	1.934	1.809	1.812	1.844
μ (mm⁻¹)	1.847	16.447	16.251	16.396	6.481	6.413	6.470
Reflections collected	13406	36565	20470	19492	19661	20824	20188
Unique reflections	6766	3989	3990	3993	3809	3860	3838
GOOF on F²	1.150	1.189	1.068	1.153	1.320	1.260	1.199
R_1 [I>2σ(I)] [a]	0.0402	0.0428	0.0500	0.0344	0.0487	0.0442	0.0613
wR_2 [I≥2σ(I)] [b]	0.0904	0.1175	0.1294	0.1026	0.1461	0.1282	0.1575
R_1 [all refl.] [a]	0.0494	0.0428	0.0525	0.0359	0.0569	0.0455	0.0637
wR_2 [all refl.] [b]	0.0947	0.1175	0.1310	0.1034	0.1533	0.1289	0.1585
R_{int}	0.0253	0.0376	0.0469	0.0334	0.0377	0.0277	0.0512

[a] $R_1 = \sum|F_o| - |F_c||/\sum|F_o|$. [b] $wR_2 = \{[\sum w(F_o^2-F_c^2)^2]/\sum[w(F_o^2)^2]\}^{1/2}$; $w = 1/[\sigma^2(F_o^2) + (aP)^2 + bP]$, where $P = [\max(F_o^2,0) + 2F_c^2]/3$ for all data.

Table S2 Selected distances (Å) and angles (°) of Cu_3L_3 complexes.

Cu₃L₃			
distance		angle	
Cu(1)−N(2)	1.853(3)	N(3)−Cu(1)−N(2)	175.53(14)
Cu(1)−N(3)	1.850(3)	N(5)−Cu(2)−N(4)	176.78(14)
Cu(2)−N(4)	1.857(3)	N(6)−Cu(3)−N(1)	176.81(14)
Cu(2)−N(5)	1.852(3)		
Cu(3)−N(1)	1.867(3)		
Cu(3)−N(6)	1.865(3)		
Cu−Cu (between Cu₃L₃)	3.080(5) 3.571(2)		

Table S3 Selected distances (Å) of the **G@X** complexes.

	B@I	B@Br	MB@I	MB@Br	TPB@I	TPB@Br
$Cu_2X_2(QT)_2$						
Cu(1)–Cu(1)#1	2.6766(2)	2.6859(1)	2.6639(2)	2.6798(1)	2.6476(1)	2.6527(2)
Cu(1)–X(1)	2.6047(9)	2.4282(9)	2.5775(10)	2.4271(9)	2.6099(7)	2.4311(13)
Cu(1)–X(2)	2.5801(8)	2.4662(9)	2.6038(10)	2.4638(9)	2.5828(7)	2.4662(13)
Cu(1)–N(1)	2.0537(1)	2.0460(1)	2.0618(2)	2.0516(1)	2.0572(1)	2.0503(2)
Cu(1)–S(1)	2.3609(13)	2.3230(13)	2.3608(16)	2.3233(13)	2.3527(11)	2.3198(17)
Cu_3Pz_3						
Cu(2)–N(2)	1.8555(1)	1.8567(1)	1.8488(2)	1.8586(1)	1.8522(1)	1.8509(2)
Cu(2)–N(3)#2	1.8522(1)	1.8634(1)	1.8536(2)	1.8560(1)	1.8543(1)	1.8482(2)
Cu(2)–Cu(1)#2	3.2228(2)	3.2227(2)	3.2241(3)	3.2264(1)	3.2120(2)	3.2139(4)
Cu–Cu(intercage)	3.7063(2)	3.7204(2)	3.6280(4)	3.6181(1)	3.7469(2)	3.7572(4)
Cu–Cu(intracage)	7.0873(4)	6.8197(4)	7.1977(8)	6.9973(3)	7.0545(4)	6.8049(8)
Symmetry code: #1 +x, +y, 1/2–z; #2 –y, +x–y, +z						

Table S4 Selected bond angles (°) of the **G@X** complexes.

	B@I	B@Br	MB@I	MB@Br	TPB@I	TPB@Br
$Cu_2X_2(QT)_2$						
X(1)−Cu(1)−X(2)	116.32(3)	111.03(3)	117.17(3)	112.18(3)	118.02(2)	113.02(4)
S(1)−Cu(1)−X(1)	105.45(4)	128.47(5)	125.51(5)	127.84(5)	103.90(3)	127.97(6)
S(1)−Cu(1)−X(2)	125.40(4)	106.55(4)	103.85(5)	104.99(4)	124.70(4)	104.83(6)
N(1)−Cu(1)−X(1)	111.03(11)	111.25(11)	110.23(14)	111.19(11)	111.85(10)	109.59(15)
N(1)−Cu(1)−X(2)	109.55(11)	110.88(11)	110.79(14)	112.01(11)	108.74(10)	112.44(15)
N(1)−Cu(1)−S(1)	84.53(12)	85.74(11)	84.51(14)	85.76(11)	84.85(10)	85.97(15)
Cu_3Pz_3						
N(2)−Cu(2)−N(3)#2	176.5(2)	176.54(18)	175.8(2)	175.71(18)	177.39(16)	177.7(2)
Symmetry code: #1 +x, +y, 1/2−z; #2 −y, +x−y, +z						

Table S5 Selected distances (Å) of TPM molecules

			B@I	B@Br	MB@I	MB@Br	TPB@I	TPB@Br	MB@S [a]
S–S		edge	11.0104(7)	11.0021(1)	11.0123(5)	11.0145(7)	11.0192(7)	11.0241(1)	10.5~10.8
		column	5.8278(4)	5.8784(7)	5.7414(3)	5.9272(4)	5.6538(3)	5.7450(7)	5.3~5.4
Cu–Cu		$intra$-Cu$_3$Pz$_3$	3.2228(2)	3.2227(2)	3.2241(3)	3.2264(1)	3.2120(2)	3.2139(4)	3.09~3.23
		$intra$-cage	7.0873(4)	7.1977(8)	6.9973(3)	7.0545(4)	6.8197(4)	6.8049(8)	6.461~6.572
		$inter$-cage (between Cu$_3$L$_3$)	3.7063(2)	3.7204(2)	3.6280(4)	3.6181(1)	3.7469(2)	3.7572(4)	2.901
Q1-Q2 [b]			7.6255(5)	7.6400(5)	7.5767(9)	7.6036(4)	7.5487(5)	7.5927(9)	5.4463(2) 5.3763(1) [c]

[a] crystal data is referred in our previous report: Z.-C. Shi, D.-X. Zhang, S.-Z. Zhan, M. Li, J. Zheng, H. Yang, X.-P. Zhou, Isr. J. Chem., 2019, 59, 317.

[b] Q1: the center of six Cu atoms in a TPM molecule. Q2: the center of Cu$_2$X$_2$ in a TPM molecule. Q1 and Q2 are shown in Fig. S4.

[c] Q2 is the S atom in thiophene groups.

Section 3: Additional Structural Description

3.1 ^{1}H NMR and PXRD
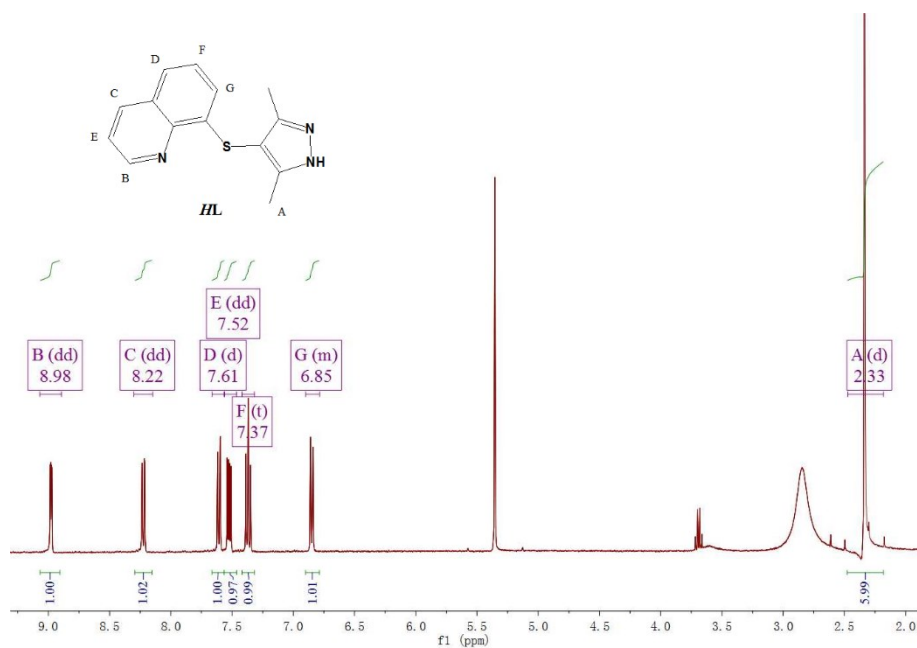
Fig. S1 ^{1}H NMR of the ligand HL in CD$_2$Cl$_2$.
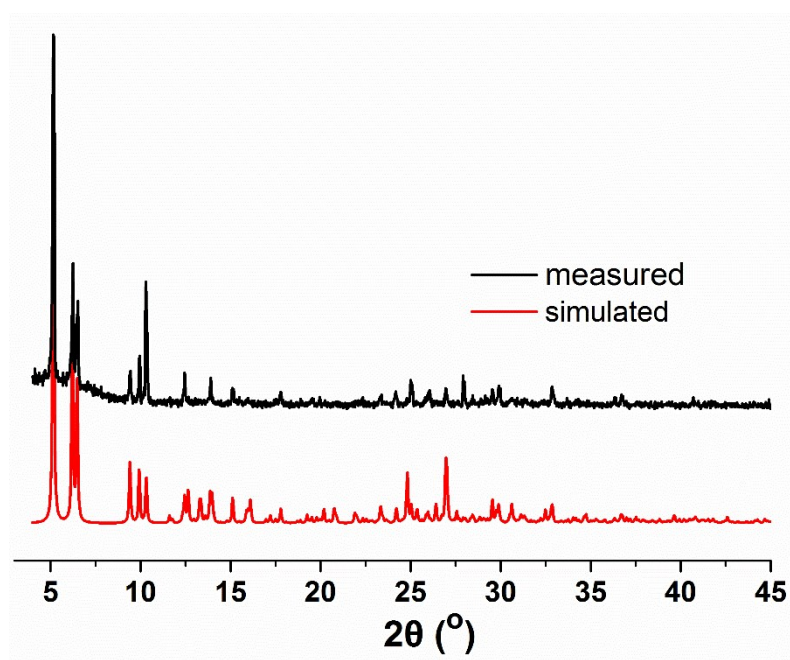
(a) Cu$_3$L$_3$
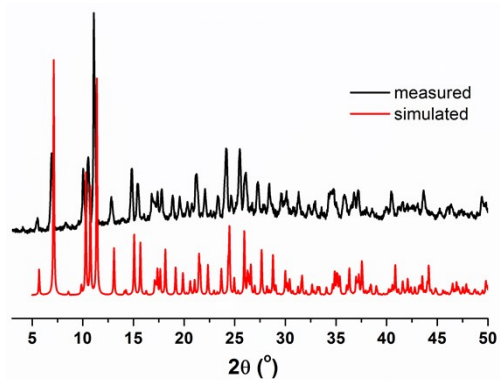
(b) **B@I**
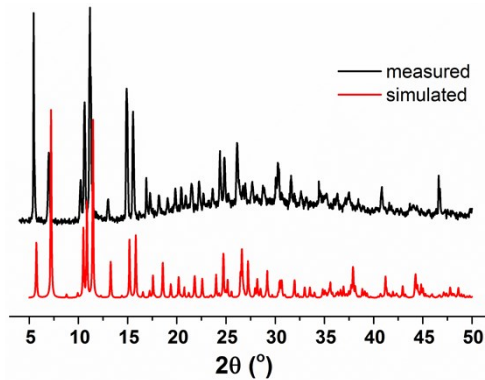
(c) **B@Br**
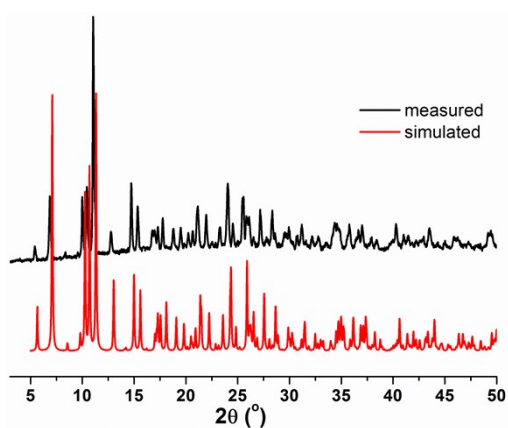
(d) **MB@I**
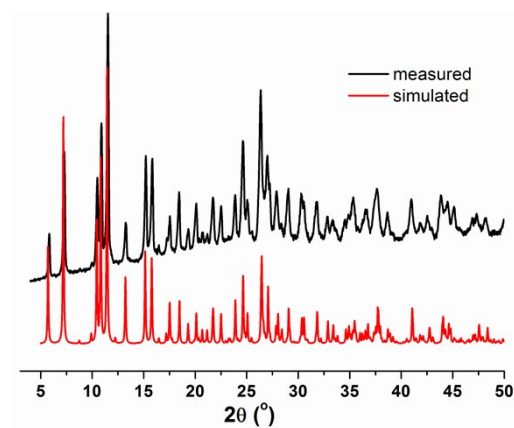
(e) **MB@Br**
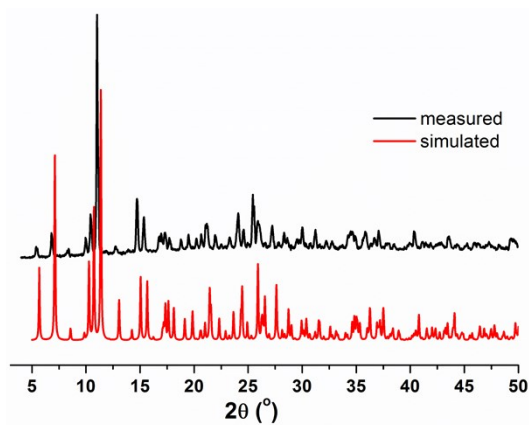
(f) **TPB@I**
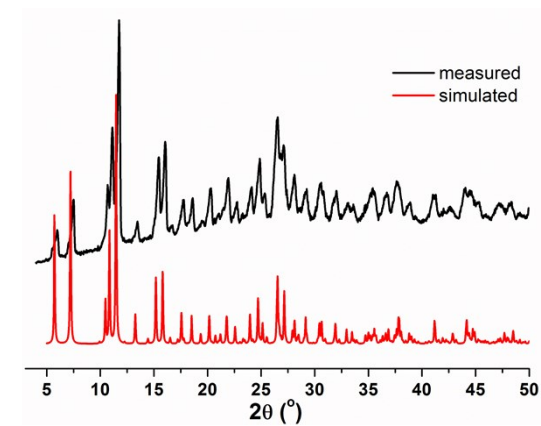
(g) **TPB@Br**

Fig. S2 Comparison of the measured and simulated PXRD patterns of Cu_3L_3 and **G@X** TPMs.

3.2 Structural Description
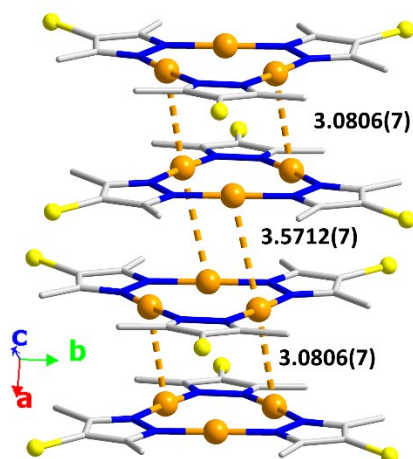
Fig. S3 Intertrimeric Cu⋯Cu interactions of Cu$_3$L$_3$ complex (Quinolinyl and methyl groups are omitted for clarity. Color codes: orange, Cu; blue, N; yellow, S; gray, C).
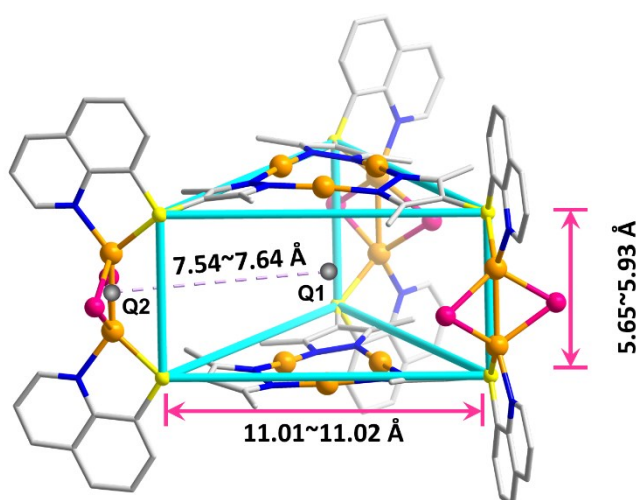
Fig. S4 Illustration of the inner size of these TPM molecules by taking the **B@I** TPM as example. (Color codes: orange, Cu; blue, N; yellow, S; gray, C; purple, I)

| (a) | (b) | (c) |
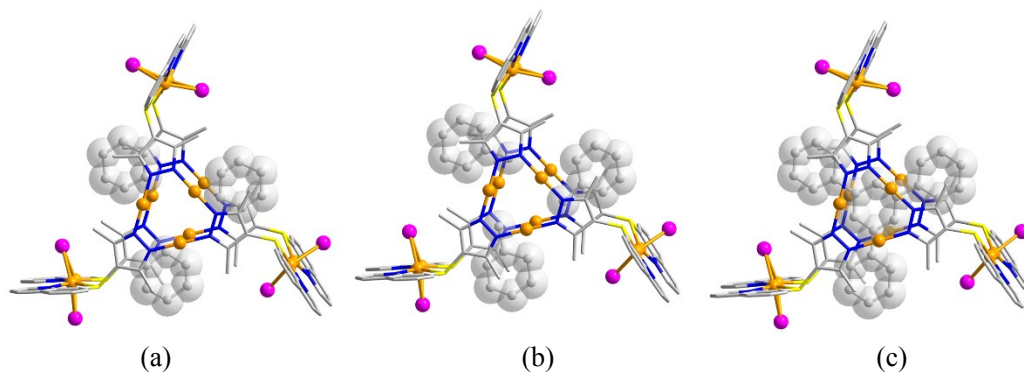
Fig. S5 Molecular structures of the **G@Br** TPMs. (a) **B@Br**; (a) **MB@Br**; (a) **TPB@Br**. The guest molecules are depicted as space-filling model. (Color codes: orange, Cu; blue, N; yellow, S; gray, C; pink, Br)
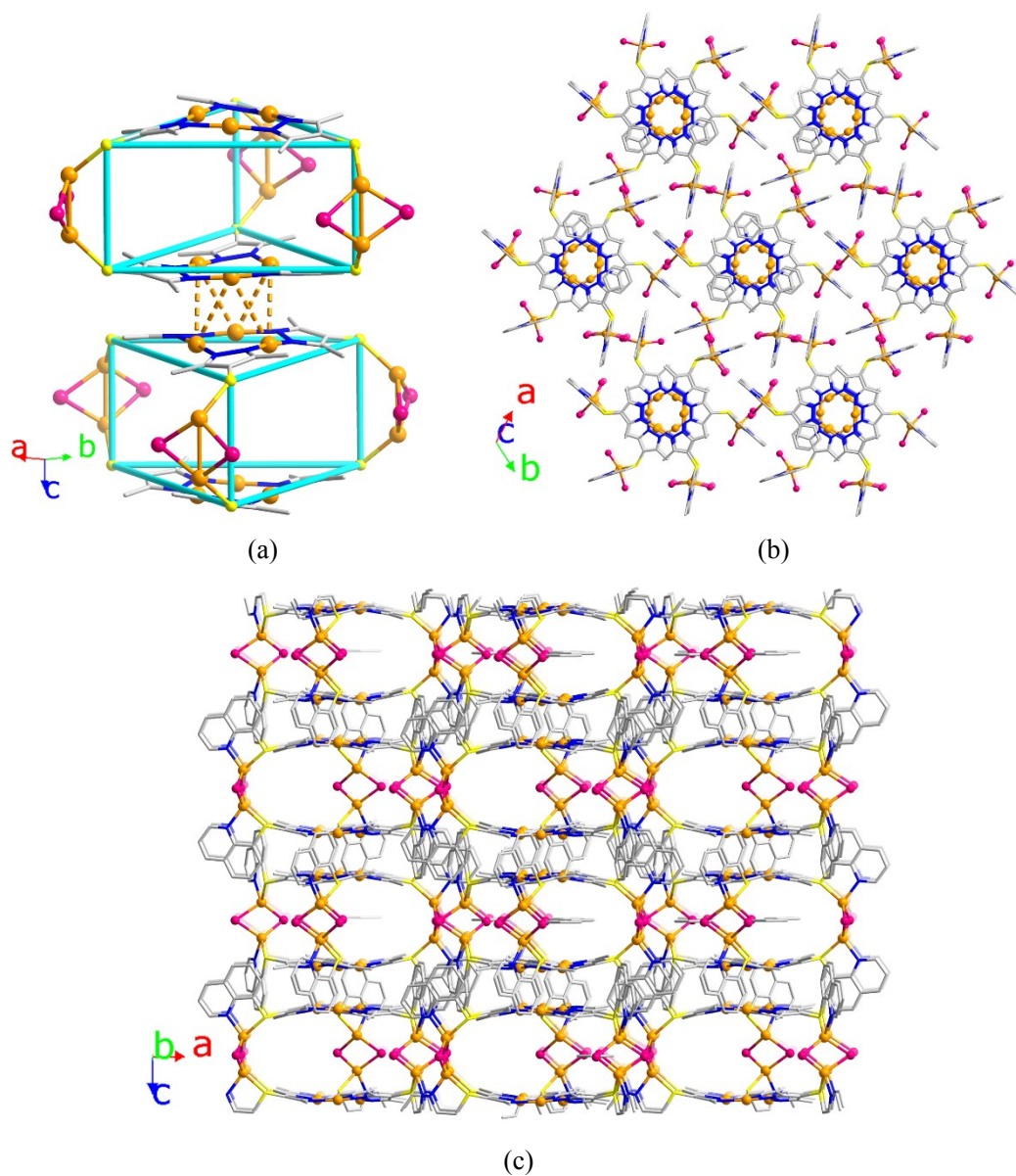
Fig. S6 Packing structures of these TPMs by taking the vacant I TPM as example. (a) 1-D supramolecular chain along c axis supported by staggered Cu···Cu interactions between adjacent TPM molecules. (b-c) packing diagrams along c (b) and b (c) axis. (Color codes: red, Cu; blue, N; yellow, S; black, C; purple, I)

3.3 Thermogravimetric analysis

(a) **B@I**

(b) **B@Br**

(c) **MB@I**

(d) **MB@Br**

(e) **TPB@I**

(f) **TPB@Br**
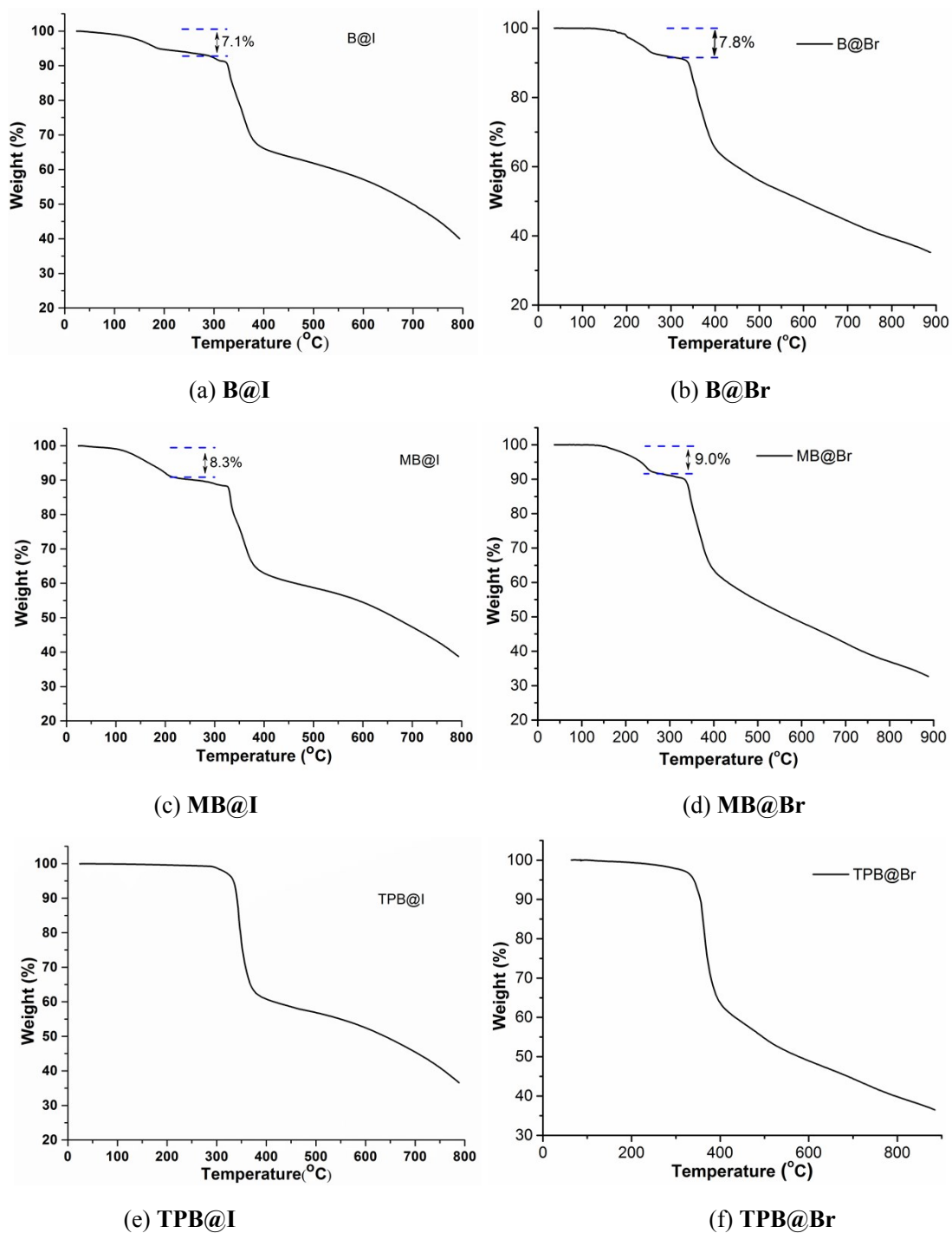
Fig. S7 Thermogravimetric plot of interlocked metallocages. The weight loss before 300 °C are in agreement with the calculated percentage of guests (7.12% in **B@I**, 7.79% in **B@Br**, 8.29% in **MB@I**, 9.06% in **MB@Br**).

Section 4: Spectra Properties

4.1 UV-Vis absorption spectra
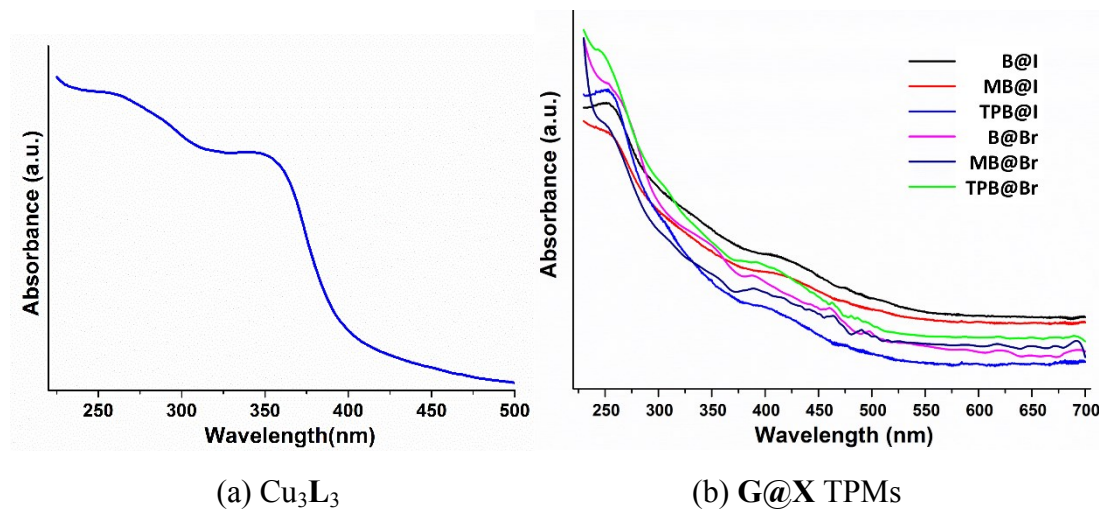
(a) Cu_3L_3

(b) **G@X** TPMs

Fig. S8 UV-Vis absorption spectra of Cu_3L_3 and **G@X** TPMs in solid state.

4.2 Photoluminescence spectra

(a)

(b)
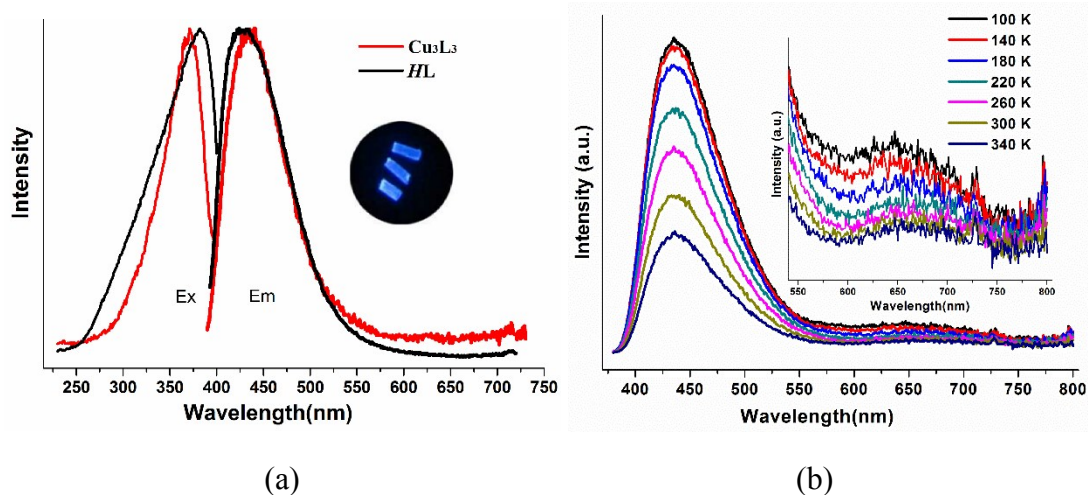
Fig. S9 (a) Solid photoluminescence spectra of the ligand *H*L and Cu_3L_3 complex at room temperature (inset image: crystal photograph of Cu_3L_3 complex under 365 nm UV light). (b) Temperature-dependent photoluminescence spectra from 100 to 340 K of Cu_3L_3 complex with 360 nm excitations.
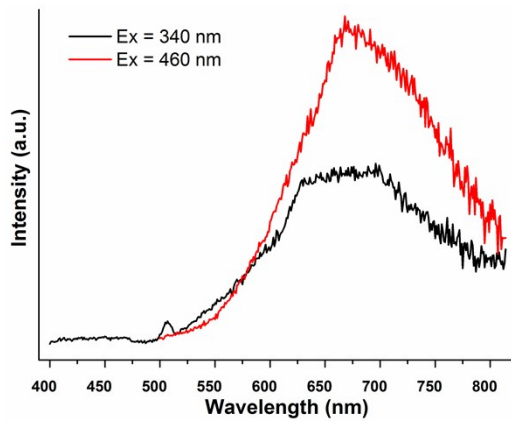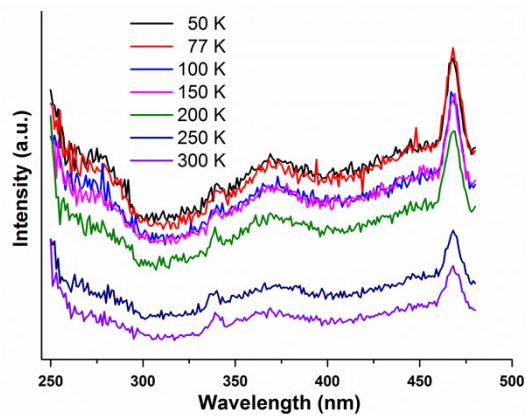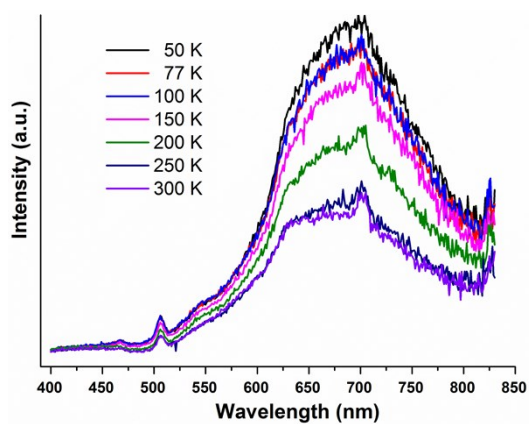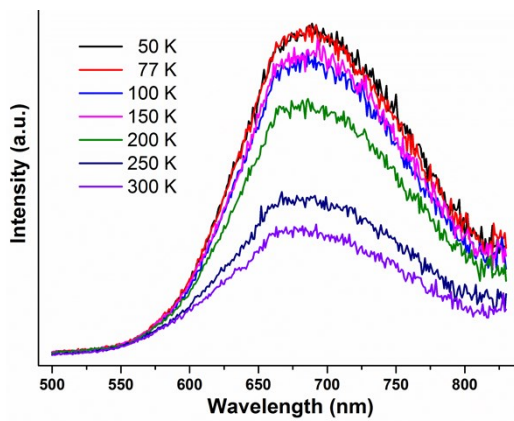
Fig. S10 Photoluminescence spectra of **B@I** TPMs in solid state.

(a) Emission spectra excited by 340 and 460 nm at room temperature.

(b) Excitation spectra monitored by 680 nm under various temperatures.
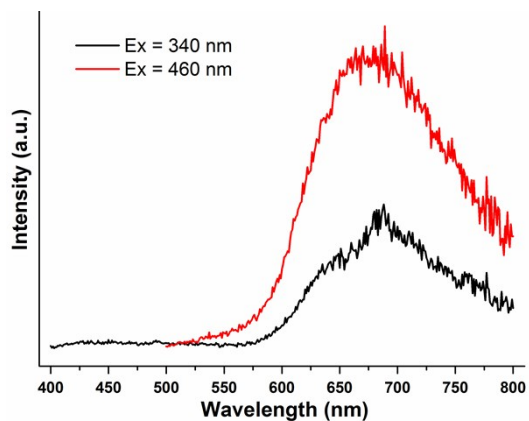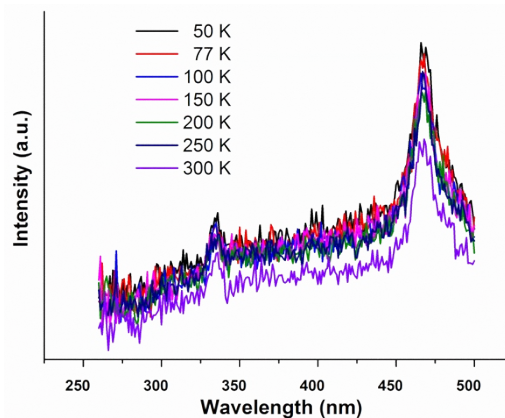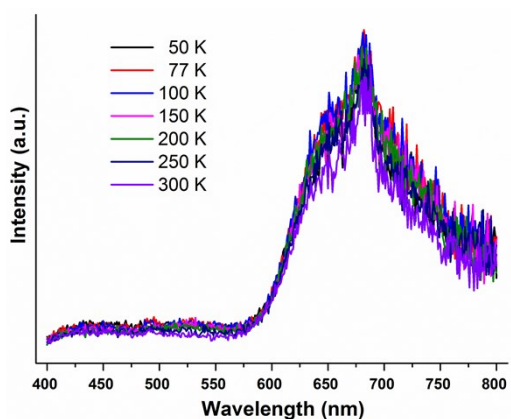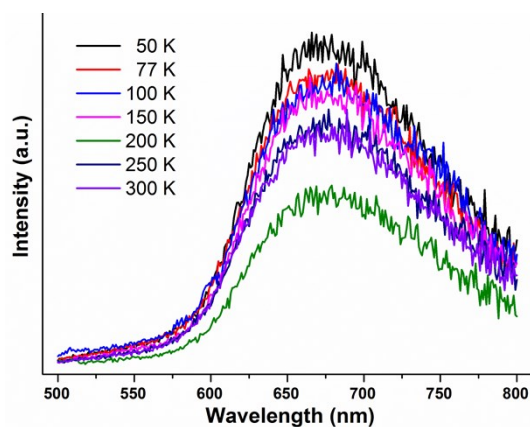
(c-d) Emission spectra under various temperatures excited by 340 (c) and 460 nm (d).

Fig. S11 Photoluminescence spectra of **B@Br** TPMs in solid state.

(a) Emission spectra excited by 340 and 460 nm at room temperature.

(b) Excitation spectra monitored by 675 nm under various temperatures.

(c-d) Emission spectra under various temperatures excited by 340 (c) and 460 nm (d).
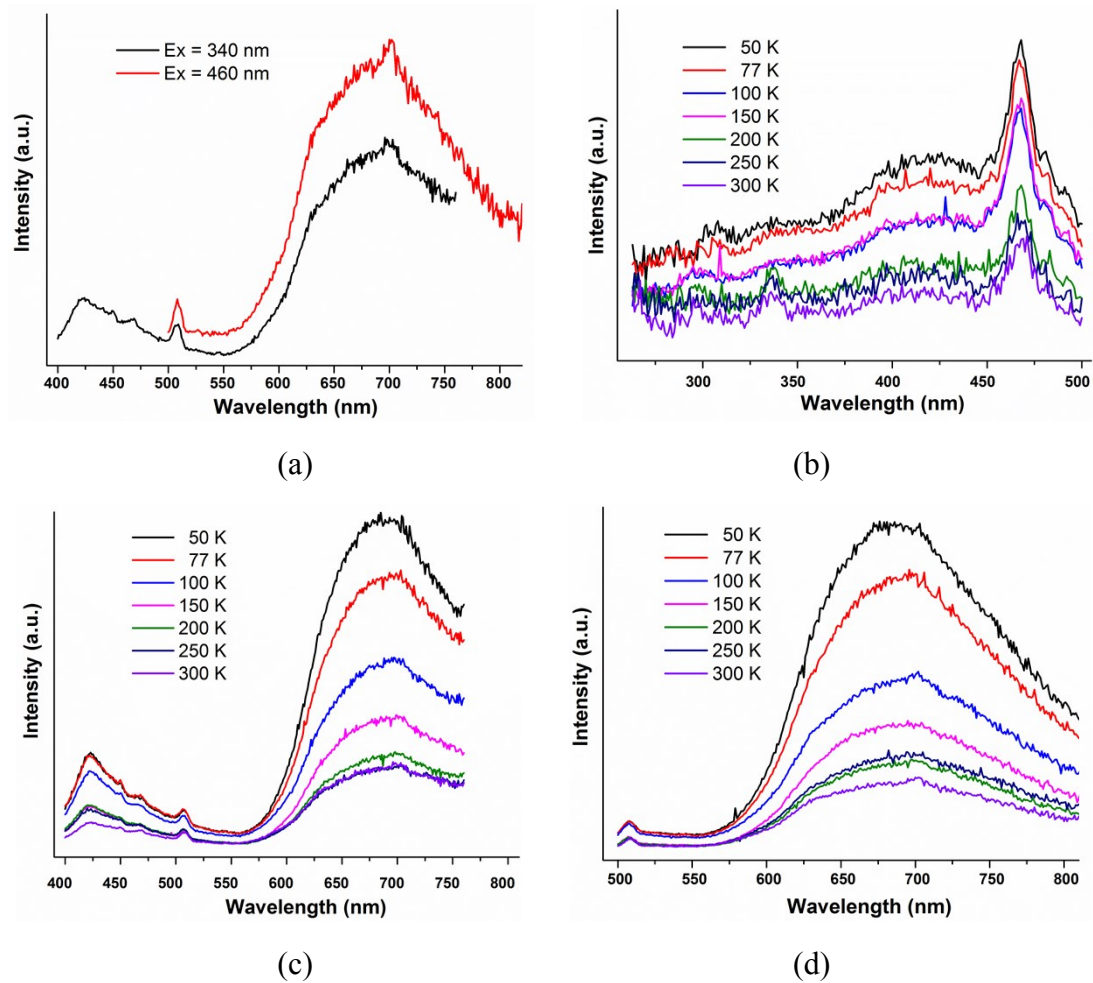
Fig. S12 Photoluminescence spectra of **MB@I** TPMs in solid state.
(a) Emission spectra excited by 340 and 460 nm at room temperature.
(b) Excitation spectra monitored by 680 nm under various temperatures.
(c-d) Emission spectra under various temperatures excited by 340 (c) and 460 nm (d).
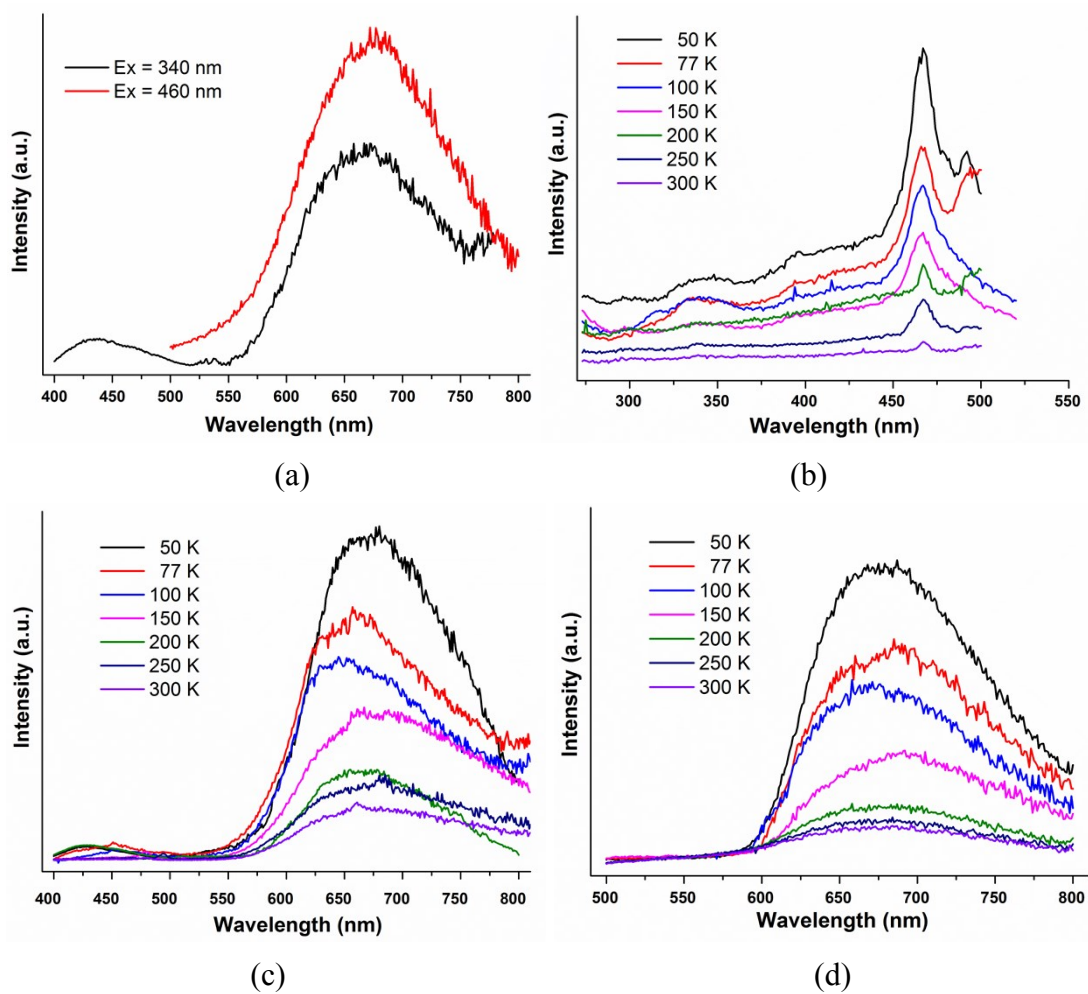
Fig. S13 Photoluminescence spectra of **MB@Br** TPMs in solid state.

(a) Emission spectra excited by 340 and 460 nm at room temperature.

(b) Excitation spectra monitored by 675 nm under various temperatures.

(c-d) Emission spectra under various temperatures excited by 340 (c) and 460 nm (d).
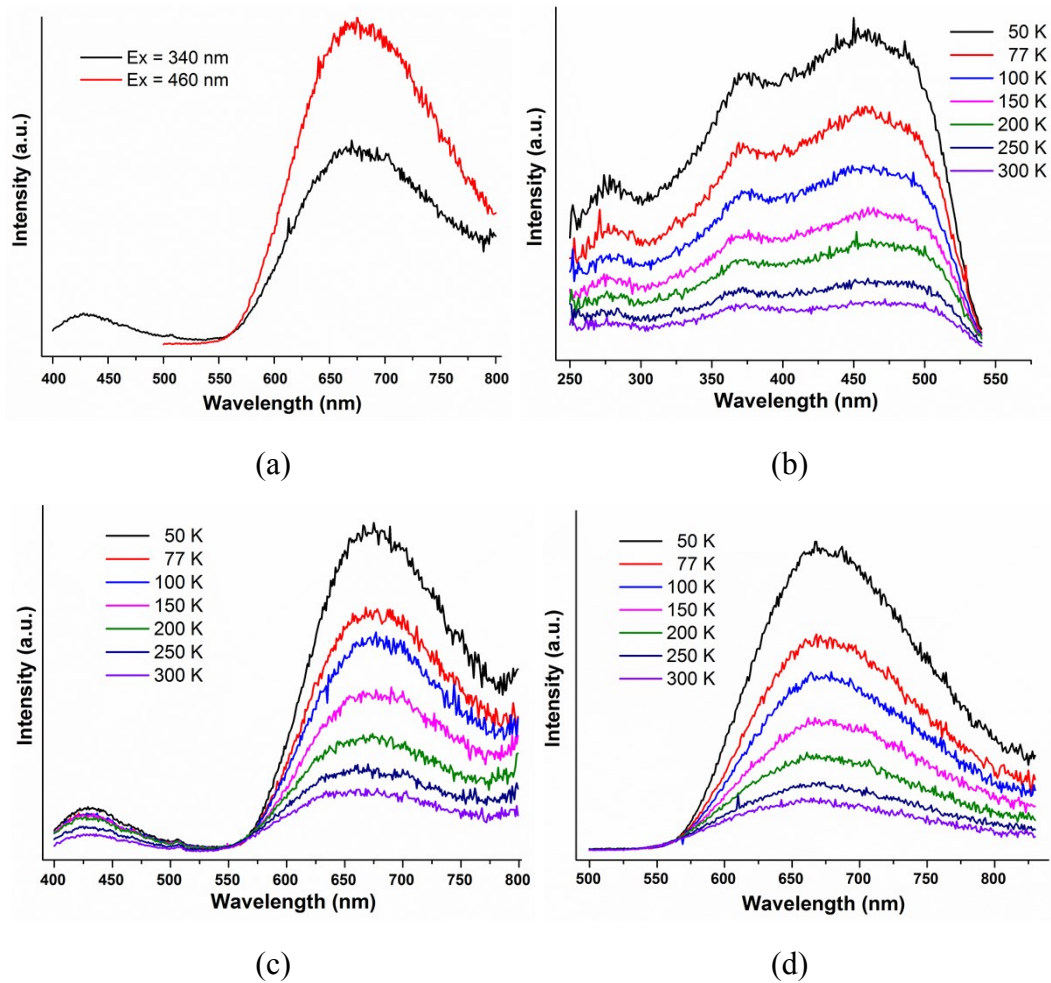
Fig. S14 Photoluminescence spectra of **TPB@I** TPMs in solid state.

(a) Emission spectra excited by 340 and 460 nm at room temperature.

(b) Excitation spectra monitored by 680 nm under various temperatures.
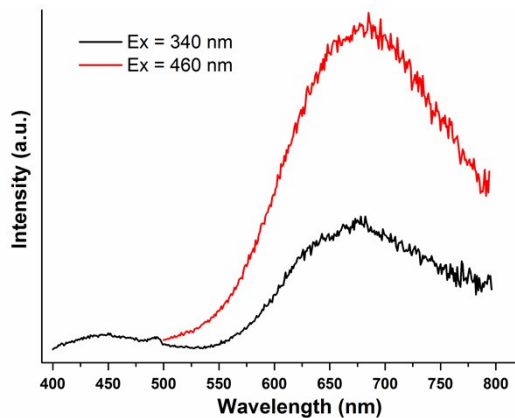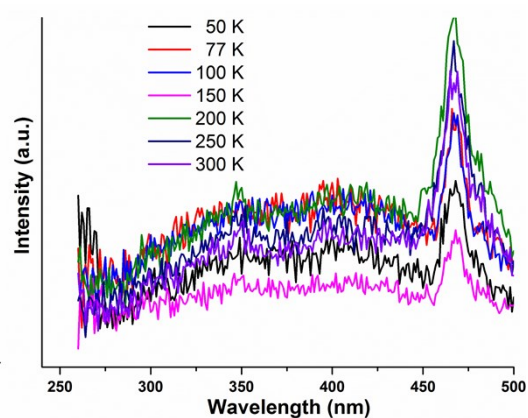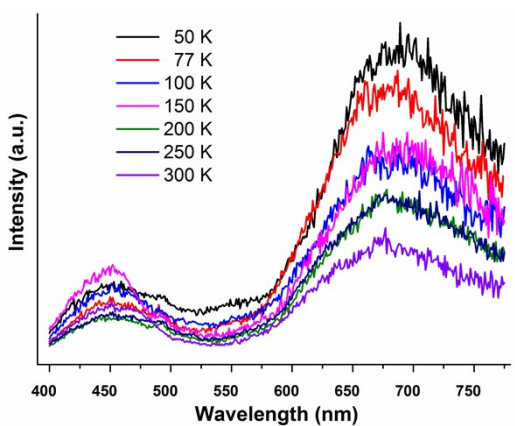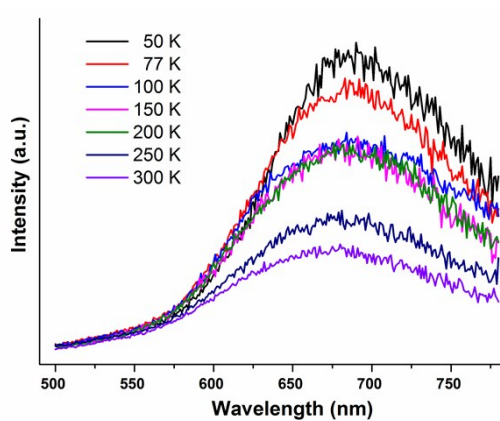
(c-d) Emission spectra under various temperatures excited by 340 (c) and 460 nm (d).

Fig. S15 Photoluminescence spectra of **TPB@Br** TPMs in solid state.

(a) Emission spectra excited by 340 and 460 nm at room temperature.

(b) Excitation spectra monitored by 675 nm under various temperatures.

(c-d) Emission spectra under various temperatures excited by 340 (c) and 460 nm (d).

Section 5: Computational Details

5.1 EDA calculation

To make a further comprehend into the nature of host-guest interactions in these TPM molecules, we evaluated the energy of the interaction (ΔE_{int}) in the TPM molecules in terms of different chemically meaningful quantities with energy decomposition analysis (EDA) proposed by Ziegler and Rauk.[S5-S7] ΔE_{int} can be decomposed into four quantities according to: $\Delta E_{int} = \Delta E_{Pauli} + \Delta E_{elstat} + \Delta E_{orb} + \Delta E_{disp}$, where the ΔE_{Pauli} part concerns the nature of destability owing to the four-electron/two-orbital repulsion between occupied orbitals between host and guest. The ΔE_{elstat} and ΔE_{orb} interpret the favorable electrostatic and covalent character of the interaction. Furthermore, the dispersion interaction (ΔE_{disp}) was evaluated via the pairwise correction of Grimme[S8] (DFT-D3), indicating a stabilizing character. And the EDA calculation was performed using the ADF2016 code.[S9-S10] Triple-ξ and one polarization functions (STO-TZP) basis sets were employed within the generalized gradient approximation (GGA) of BLYP exchange−correlation functional. The pair-wise Grimme correction (D3)[S11-S14] and Becke−Johnson damping functions[S15-S16] were considered for the empirical dispersion correction to density functional theory (DFT-D). The crystal molecular structure was used for calculation.

The molecular structures of **B@S** and **MB@S** in our previous report [S17] were used as calculation models to compare host-guest interactions with the titled TPM molecules. It is noted that molecular structure of **B@S** is derived from the **MB@S** by replacing the CH_3 in **MB** with H atom.

5.2 Density Functional Theory (DFT) and Time-Dependent Density Functional Theory (TDDFT) Calculations
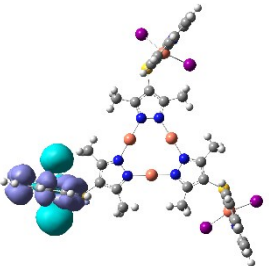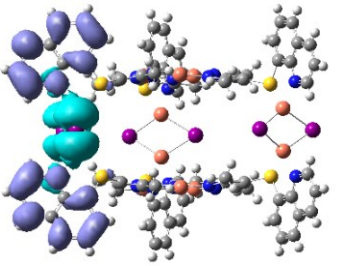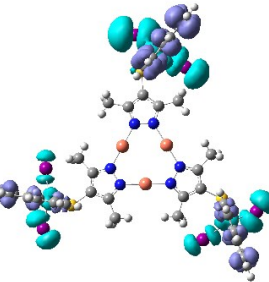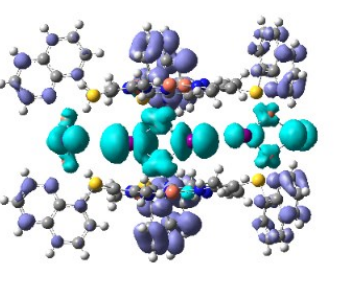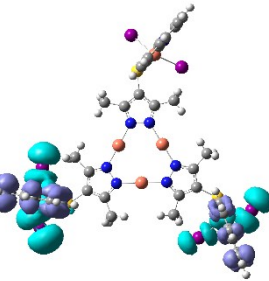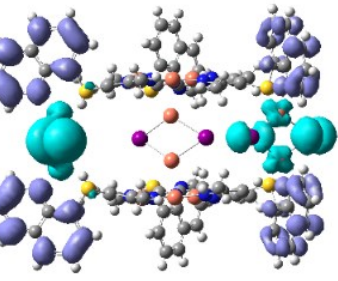
Calculated models of both single metallocage and dimeric metallocage was taken from the X-ray data of **B@I** at 100 K. Since either UV-Vis absorption spectra or photoluminescence spectra seem to be insensitive to the encapsulated guest molecules, the vacant metallocage without any guest molecules was used for calculations so as to reduce calculation cost.
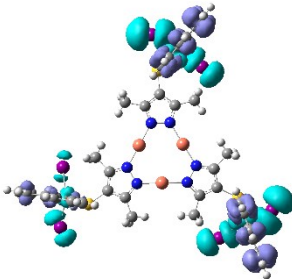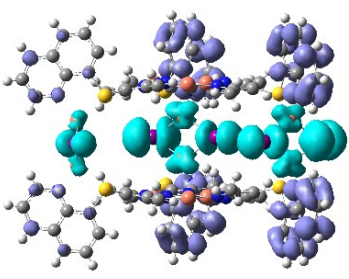
Molecular orbital calculations were carried out for both single cage and its dimer, and the first 30 $S_0 \rightarrow S_n$ spin-allowed transitions were also calculated for the single cage with IOP(9/40=4). All calculation were performed using PBE0 functional[S18] in Gaussian 09 package[S19] with Lanl2dz effective core potential[S20] (ECP) for Cu as well as I atoms and 6-31G** basis set[S21] for other atoms. The cub files for drawing contours of orbitals (isovalue = 0.02) and electron density difference (EDD) maps (isovalue = 5.0×10^{-4} a.u.) were obtained by Multiwfn 3.5[S22] using formatted checkpoint files (fchk) and/or Guassian output files (log). The EDD maps for S_n state with oscillator strength (f) lower than 0.01 have not been provided, except for S_1 state.

Table S6 The calculated first 30 transitions based on the S_0 state.

No.	singlet-singlet spin-allowed transition			singlet-triplet spin-forbidden transition	
	E/eV	λ/nm	f	E/eV	λ/nm
1	2.253	550.7	0.0000	2.165	573.0
2	2.254	550.6	0.0000	2.166	572.8
3	2.254	550.4	0.0000	2.166	572.8
4	2.259	549.2	0.0012	2.166	572.8
5	2.260	549.0	0.0012	2.167	572.7
6	2.260	548.9	0.0013	2.167	572.6
7	2.524	491.5	0.0000	2.254	550.4
8	2.525	491.5	0.0000	2.254	550.4
9	2.525	491.3	0.0000	2.255	550.3
10	2.528	490.9	0.0015	2.255	550.3
11	2.528	490.8	0.0013	2.255	550.3
12	2.529	490.7	0.0007	2.255	550.2
13	2.613	474.9	0.0020	2.473	501.7
14	2.613	474.9	0.0096	2.473	501.7
15	2.615	474.5	0.1364	2.474	501.5
16	2.632	471.4	0.0191	2.474	501.5
17	2.633	471.3	0.0184	2.474	501.4
18	2.634	471.0	0.0011	2.475	501.3
19	2.828	438.8	0.0000	2.745	452.1
20	2.829	438.5	0.0000	2.745	452.0
21	2.830	438.4	0.0000	2.745	452.0
22	2.833	437.9	0.0000	2.745	451.9
23	2.834	437.8	0.0000	2.746	451.9
24	2.835	437.7	0.0000	2.746	451.8
25	2.835	437.7	0.0000	2.828	438.8
26	2.836	437.6	0.0000	2.829	438.5
27	2.836	437.5	0.0000	2.830	438.4
28	2.840	436.9	0.0000	2.833	437.9
29	2.841	436.7	0.0000	2.834	437.8
30	2.841	436.7	0.0000	2.835	437.7

Table S7 The calculated absorption spectra, the electron density difference (EDD) maps and the orbital transitions of the selected vertical singlet excited states with $f > 0.01$ at TD-PBE0/(Lanl2dz+6-31G**) level (isovalue for EDD is 5.0×10^{-4} a.u.).
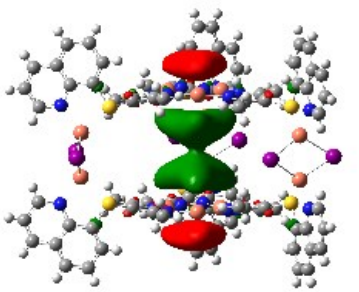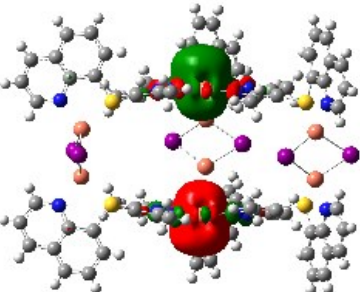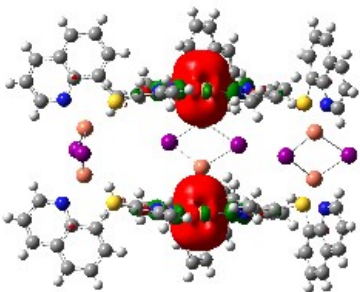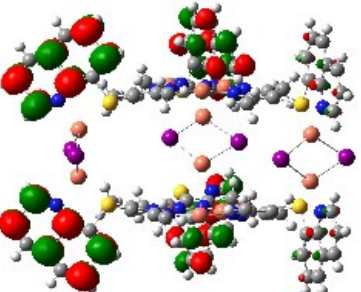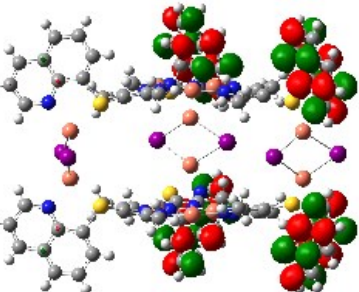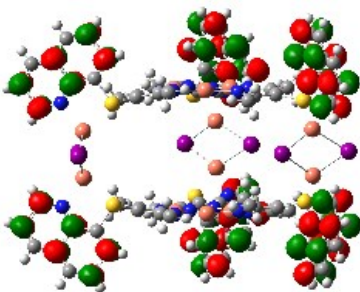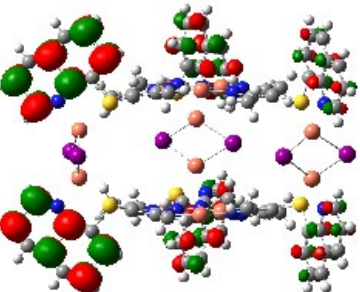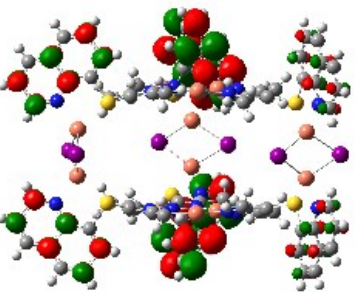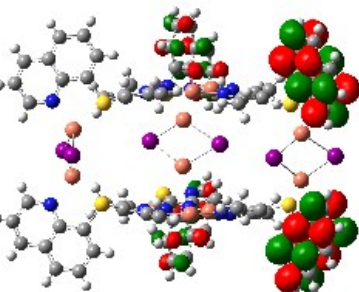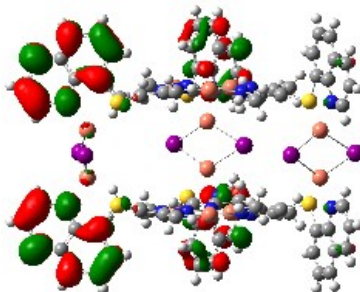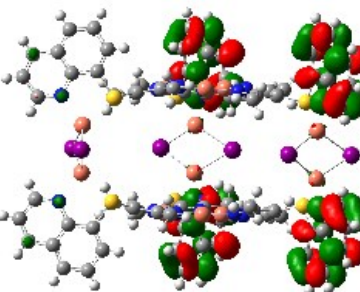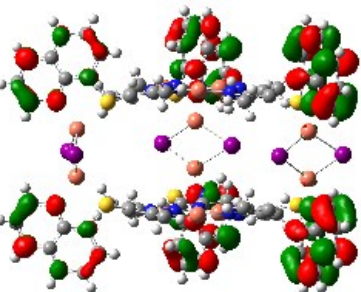
No.	E(eV)	λ(nm)	f	EDD		Major transitions and contributions (H = HOMO, L = LUMO)	Type
				Top view	Side view		
1	2.253	550.7	0.0000			H→L+5 (69.1653%) H→L+3 (19.3467%)	MLCT XLCT
15	2.615	474.5	0.1364			H-4→L+1 (21.78%) H-5→L (20.52%) H-7→L+1 (13.94%)	MLCT XLCT
16	2.632	474.5	0.0191			H-3→L+3 (17.01%) H-3→L+5 (16.93%) H-5→L+5 (15.48%)	MLCT XLCT

| 17 | 2.633 | 471.3 | 0.0184 | | | H-4→L+3 (22.16%)
 H-5→L+4 (18.53%)
 H-7→L+3 (11.96%) | MLCT
 XLCT |
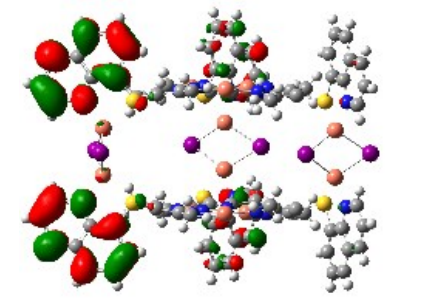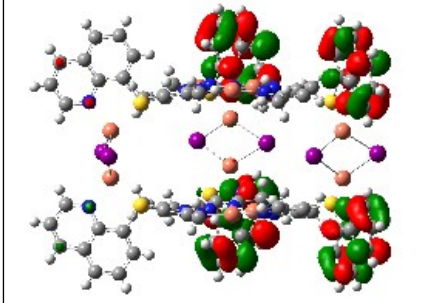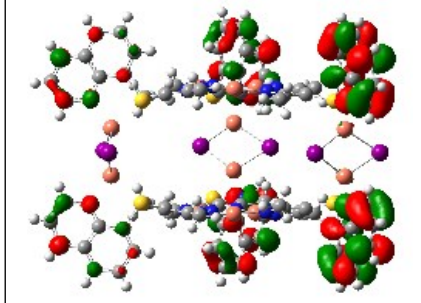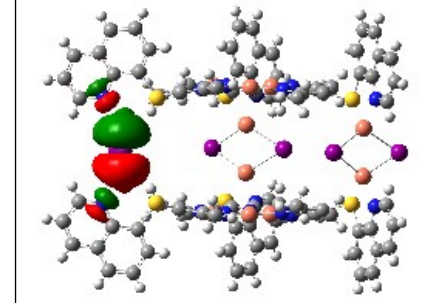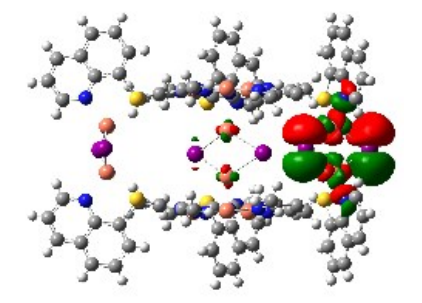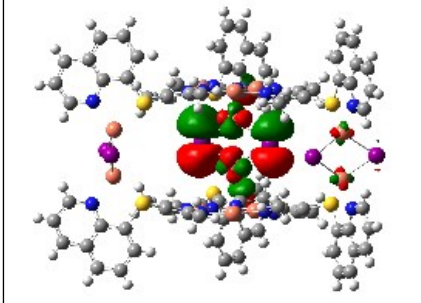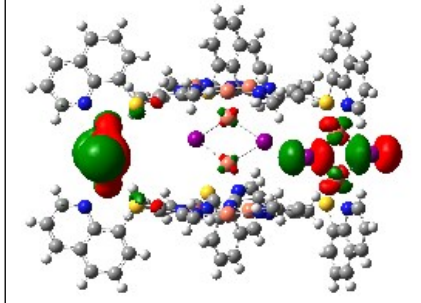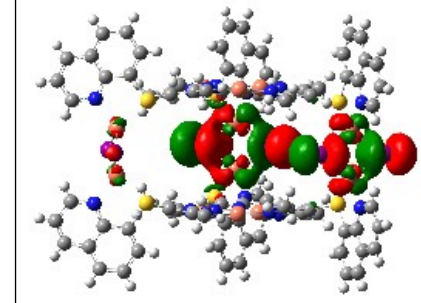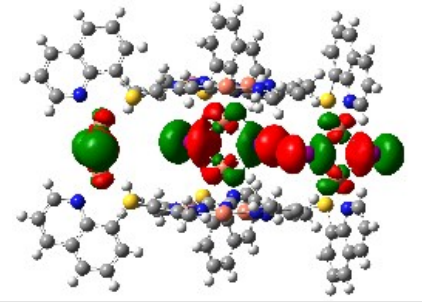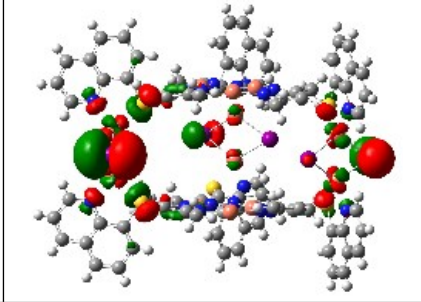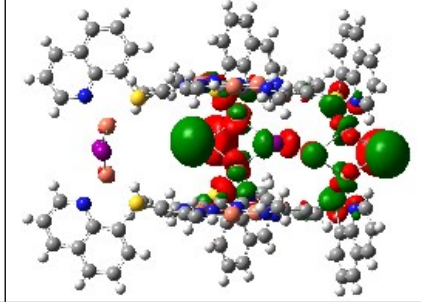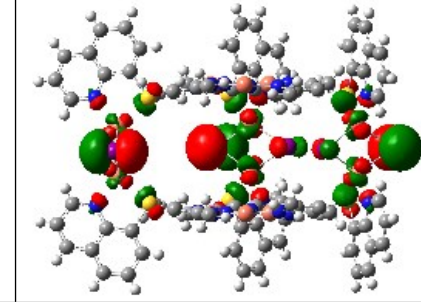
Table S8 The Hirshfeld compositions (%) of selected MOs in the ground state at the PBE0 level of theory for the TPM complexes.

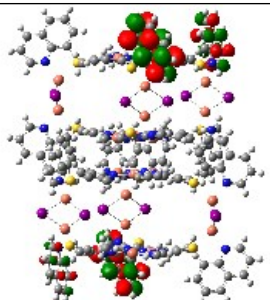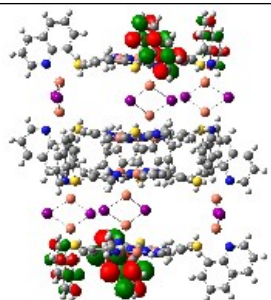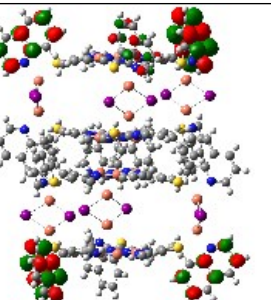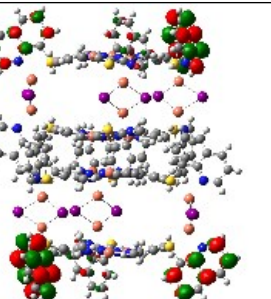| units	atoms	H-8	H-7	H-6	H-5	H-4	H-3	H-2	H-1	H	L	L+1	L+2	L+3	L+4	L+5
Cu_2I_2	Cu	**30.32**	**30.10**	**30.08**	**43.32**	**43.00**	**43.00**	**44.81**	**44.76**	**44.76**	1.07	1.13	1.13	1.07	1.12	1.12
	I	**48.74**	**47.54**	**47.59**	**50.73**	**49.66**	**49.67**	**47.33**	**47.38**	**47.39**	0.31	0.31	0.31	0.52	0.53	0.53
QT	C	3.17	3.59	3.58	2.68	2.51	2.51	1.29	1.29	1.29	**80.41**	**80.36**	**80.36**	**80.29**	**80.28**	**80.28**
	N	4.02	3.85	3.85	0.26	0.44	0.44	5.36	5.34	5.34	**15.55**	**15.59**	**15.59**	**15.33**	**15.39**	**15.39**
	S	9.47	9.45	9.44	1.38	1.74	1.74	0.50	0.51	0.51	1.28	1.28	1.28	1.34	1.34	1.34
Cu_3Pz_3	Cu	0.15	0.54	0.54	0.08	0.17	0.17	0.03	0.03	0.03	0.19	0.11	0.11	0.21	0.12	0.12
	C	3.00	3.37	3.37	1.29	1.90	1.90	0.33	0.33	0.33	0.59	0.58	0.58	0.62	0.59	0.59
	N	0.84	1.27	1.27	0.19	0.50	0.50	0.07	0.07	0.07	0.05	0.06	0.06	0.04	0.05	0.05
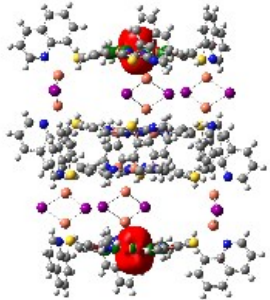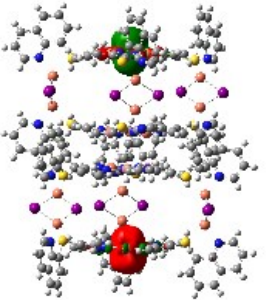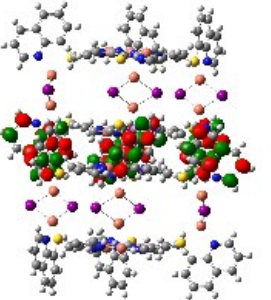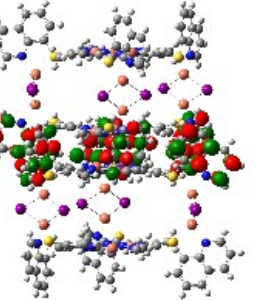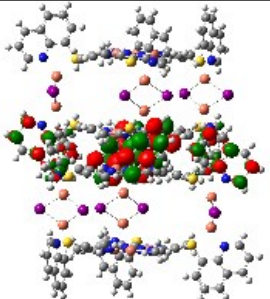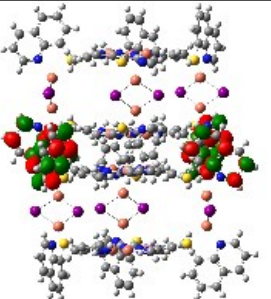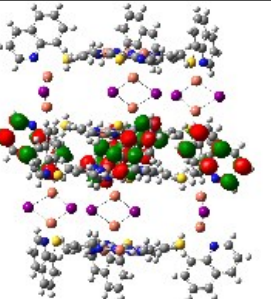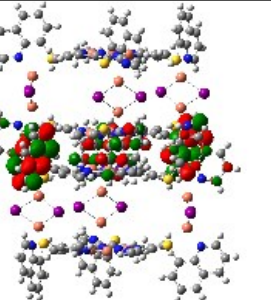
Table S9 Information of Selected MOs for the single cage at PBE0/(Lanl2dz+6-31G**) level (isovalue for orbital contours is 0.02).

Orbital Contour				
E(eV)	0.036	-0.288	-0.314	-0.639
Orb. No.	LUMO+14	LUMO+13	LUMO+12	LUMO+11
Orbital Contour				
E(eV)	-0.639	-0.640	-0.640	-0.640
Orb. No.	LUMO+10	LUMO+9	LUMO+8	LUMO+7
Orbital Contour				
E(eV)	-0.640	-1.806	-1.806	-1.807
Orb. No.	LUMO+6	LUMO+5	LUMO+4	LUMO+3
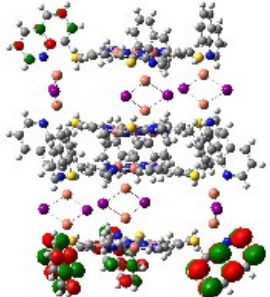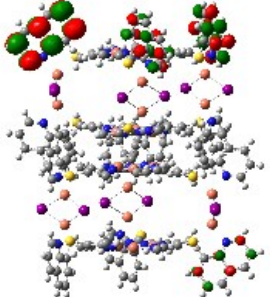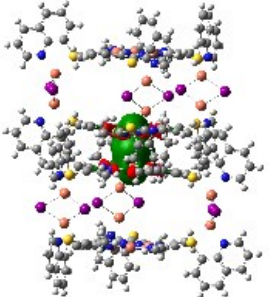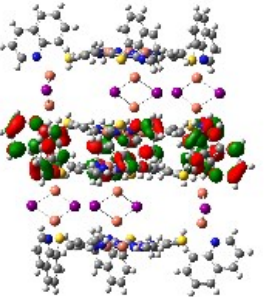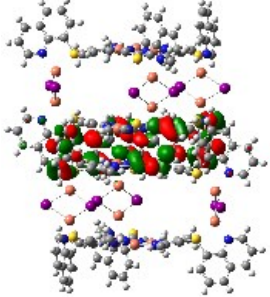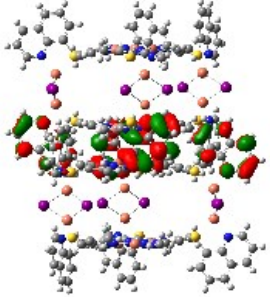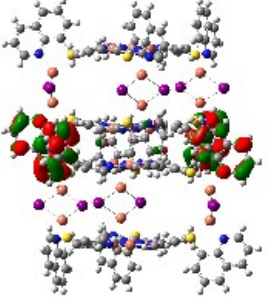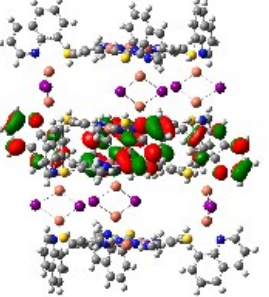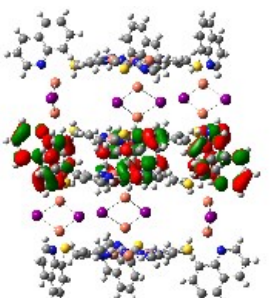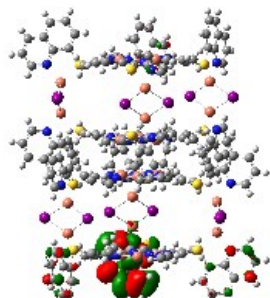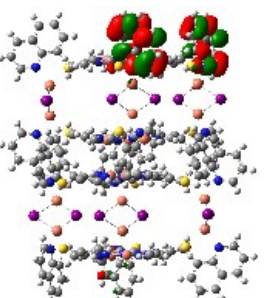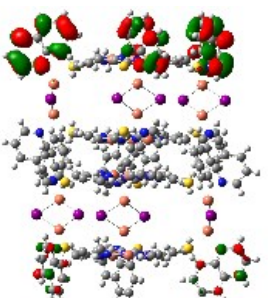
Orbital Contour			
E(eV)	-1.813	-1.813	-1.813	-4.879
Orb. No.	LUMO+2	LUMO+1	LUMO	HOMO
Orbital Contour			
E(eV)	-4.880	-4.880	-5.126	-5.126
Orb. No.	HOMO-1	HOMO-2	HOMO-3	HOMO-4
Orbital Contour			
E(eV)	-5.132	-5.186	-5.186	-5.199
Orb. No.	HOMO-5	HOMO-6	HOMO-7	HOMO-8
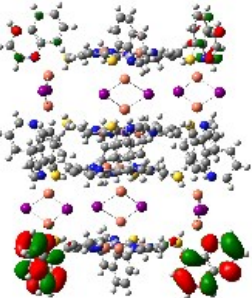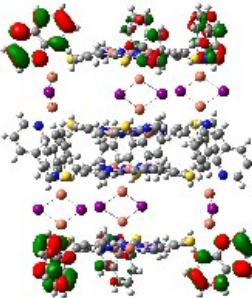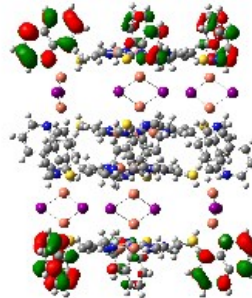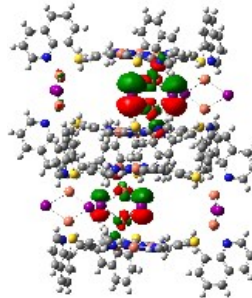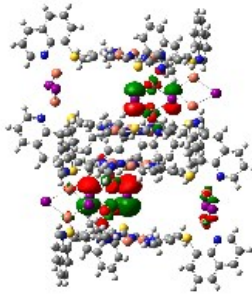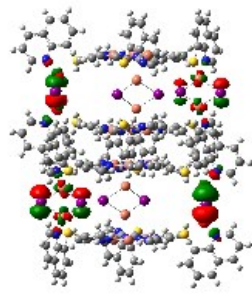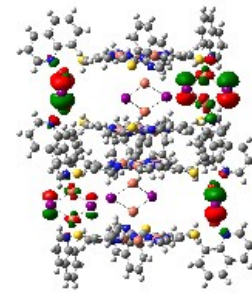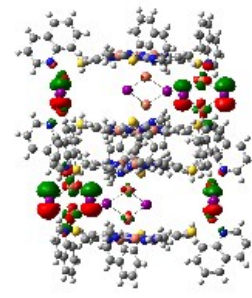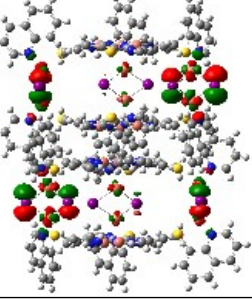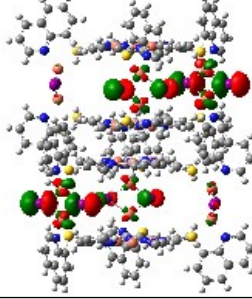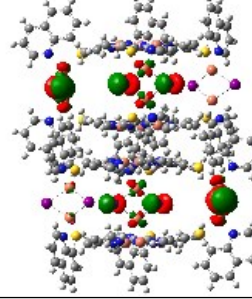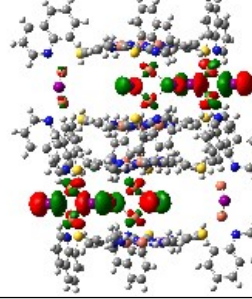
Table S10 Information of Selected MOs for the dimer of TPM at PBE0/(Lanl2dz+6-31G**) level (isovalue for orbital contours is 0.02).

Orbital Contour				
E(eV)	-0.342	-0.345	-0.570	-0.570
Orb. No.	LUMO+26	LUMO+25	LUMO+24	LUMO+23
Orbital Contour				
E(eV)	-0.571	-0.571	-0.574	-0.574
Orb. No.	LUMO+22	LUMO+21	LUMO+20	LUMO+19
Orbital Contour				
E(eV)	-0.667	-0.668	-0.668	-0.668
Orb. No.	LUMO+18	LUMO+17	LUMO+16	LUMO+15
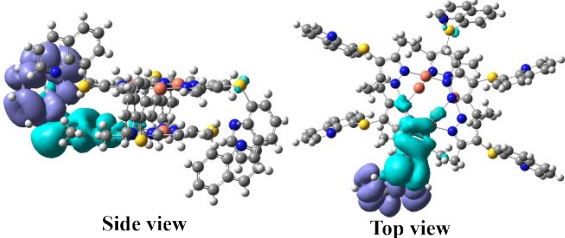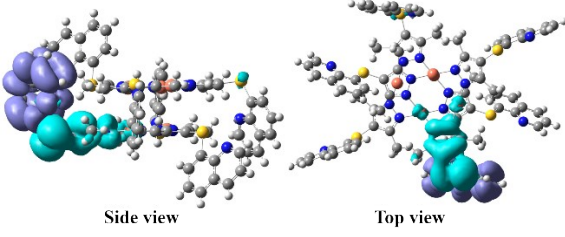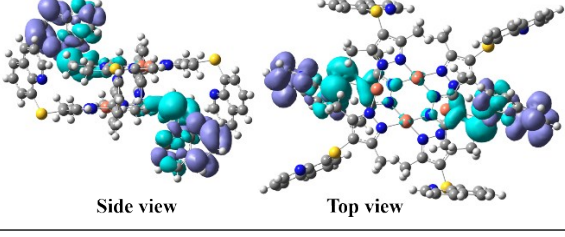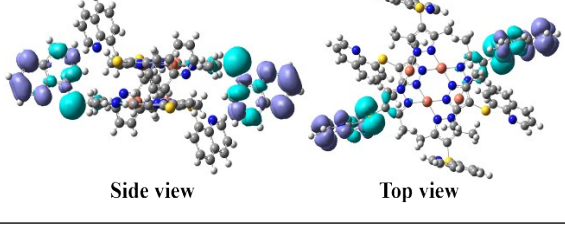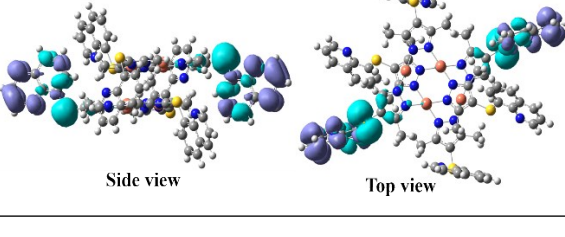
Orbital Contour				
E(eV)	-0.668	-0.668	-0.709	-1.730
Orb. No.	LUMO+14	LUMO+13	LUMO+12	LUMO+11
Orbital Contour				
E(eV)	-1.731	-1.731	-1.735	-1.735
Orb. No.	LUMO+10	LUMO+9	LUMO+8	LUMO+7
Orbital Contour				
E(eV)	-1.742	-1.837	-1.837	-1.837
Orb. No.	LUMO+6	LUMO+5	LUMO+4	LUMO+3

Orbital Contour				
E(eV)	-1.837	-1.838	-1.838	-4.898
Orb. No.	LUMO+2	LUMO+1	LUMO	HOMO
Orbital Contour				
E(eV)	-4.898	-4.898	-4.898	-4.898
Orb. No.	HOMO-1	HOMO-2	HOMO-3	HOMO-4
Orbital Contour				
E(eV)	-4.898	-5.149	-5.149	-5.150
Orb. No.	HOMO-5	HOMO-6	HOMO-7	HOMO-8

Table S11 Selected TDDFT results in the first 40 singlet-singlet spin-allowed vertical excited state for dimer of Cu_3L_3.

No	λ(nm)	E(eV)	f	EDD	Type
1	367.8	3.374	0.022	Side view · Top view	[1]ILCT, [1]MLCT
2	367.7	3.375	0.012	Side view · Top view	[1]ILCT/
3	345.9	3.587	0.209	Side view · Top view	[1]ILCT
7	338.9	3.660	0.242	Side view · Top view	[1]ILCT
8	338.7	3.663	0.002	Side view · Top view	[1]ILCT

Section 6: Reference

S1 (a) T.-J. Won, J. K. Clegg, L. F. Lindoy, J. C. McMurtrie, *Cryst. Growth Des.* 2007, **7***,* 972. (b) Z. Yoshida, H. Ogoshi, T. Tokumitsu, *Tetrahedron.* 1970, **26***,* 2987. (c) S.-Z. Zhan, W. Chen, W. Lu, J. Zheng, F. Ding, T. Feng, D. Li, *Inorg. Chem.* 2019, **58**, 1081. (d) S.-Z. Zhan, J.-H. Li, M. Li, G.-H. Zhang, X.-W. Liu, J. Zheng, S. W. Ng, D. Li, *Chem. Commun.*, 2019, 11992.

S2 G. M. Sheldrick, *Acta Crystallogr., Sect. C: Struct. Chem.*, 2015, **71**, 3.

S3 O. V. Dolomanov, L. J. Bourhis, R. J. Gildea, J. A. K. Howard, H. Puschmann, *J. Appl. Cryst.*, 2009, **42**, 339.

S4 O. V. Dolomanov, A. J. Blake, N. R. Champness, M. Schröder, *J. Appl. Crystallogr.* 2003, **36**, 1283.

S5 von Hopffgarten, M.; Frenking, G. *Wiley Interdiscip. Rev.: Comput. Mol. Sci.* 2012, **2**, 43.

S6 K. Morokuma, *J. Chem. Phys.* 1971, **55**, 1236.

S7 T. Ziegler, A. Rauk, *Theor. Chim. Acta* 1977, **46**, 1.

S8 S. Grimme, Wiley Interdiscip. Rev.: *Comput. Mol. Sci.* 2011, **1**, 211

S9 G. te Velde, E. J. Baerends, *Phys. Rev. B: Condens. Matter Mater. Phys.* 1991, **44**, 7888.

S10 C. Fonseca Guerra, J. G. Snijders, G. te Velde, E. J. Baerends, *Theor. Chem. Accounts Theor. Comput. Model.* 1998, **99**, 391.

S11 S. Grimme, *J. Comput. Chem.* 2006, **27**, 1787.

S12 S. Grimme, *J. Comput. Chem.* 2004, **25**, 1463.

S13 S. Grimme, J. Antony, S. Ehrlich, H. Krieg, *J. Chem. Phys.* 2010, **132**, 154104.

S14 S. Grimme, Wiley Interdiscip. *Rev.: Comput. Mol. Sci.* 2011, **1**, 211.

S15 E. R. Johnson, A. D. Becke, *J. Chem. Phys.* 2005, **123**, 024101.

S16 S. Grimme, S. Ehrlich, L. Goerigk, *J. Comput. Chem.* 2011, **32**, 1456.

S17 Z.-C. Shi, D.-X. Zhang, S.-Z. Zhan, M. Li, J. Zheng, H. Yang, X.-P. Zhou, *Isr. J. Chem.*, 2019, **59**, 317.

S18 (a) J. P. Perdew, K. Burke, M. Ernzerhof, *Phys. Rev. Lett.* 1996, **77**, 3865. (b) J. P. Perdew, K. Burke, M. Ernzerhof, *Phys. Rev. Lett.* 1997, **78**, 1396.

S19 M. J. Frisch, G. W. Trucks, H. B. Schlegel, G. E. Scuseria, M. A. Robb, J. R. Cheeseman, G. Scalmani, V. Barone, B. Mennucci, G. A. Petersson, H. Nakatsuji, M. Caricato, X. Li, H. P. Hratchian, A. F. Izmaylov, J. Bloino, G. Zheng, J. L. Sonnenberg, M. Hada, M. Ehara, K. Toyota, R. Fukuda, J. Hasegawa, M. Ishida, T. Nakajima, Y. Honda, O. Kitao, H. Nakai, T. Vreven, Jr. J. A. Montgomery, J. E. Peralta, F. Ogliaro, M. Bearpark, J. J. Heyd, E. Brothers, K. N. Kudin, V. N. Staroverov, R. Kobayashi, J. Normand, K. Raghavachari, A. Rendell, J. C. Burant, S. S. Iyengar, J. Tomasi, M. Cossi, N. Rega, J. M. Millam, M. Klene, J. E. Knox, J.B. Cross, V. Bakken, C. Adamo, J. Jaramillo, R. Gomperts, R. E. Stratmann, O. Yazyev, A. J.

Austin, R. Cammi, C. Pomelli, J. Ochterski, R. L. Martin, K. Morokuma, V. G. Zakrzewski, G. A. Voth, P. Salvador, J. J. Dannenberg, S. Dapprich, A. D. Daniels, O. Farkas, J. B. Foresman, J. V. Ortiz, J. Cioslowski, D. J. Fox, GAUSSIAN 09 (Revision A.02), Gaussian, Inc., Wallingford, CT, 2009

S20 P. J. Hay, W. R. Wadt, *J. Chem. Phys.* 1985, **82**, 270.

S21 J. E. Del Bene, *Chem. Phys. Lett.* 1983, **94(2)**, 213.

S22 T. Lu, F. W. J. Chen, *Comp. Chem.* 2012, **33**, 580.